Mechanistic Understanding of Excitation-Correlated Highly-Efficient Two-Photon Luminescence from Biocompatible MoS_2 Nanodots for Optimized Multicolor Cell Imaging

Jianhui Sun, Yanjuan Gu, Dang Yuan, Lei*, Siu Fung Yu, Shu Ping Lau, Wing-Tak Wong, Helen Lai-Wai Chan

Dr. J. Sun, Prof. Dr. D.Y. Lei, Prof. Dr. S.F. Yu, Prof. Dr. S.P. Lau, Prof. Dr. H.L.-W. Chan

Department of Applied Physics, The Hong Kong Polytechnic University, Hong Kong

Address correspondence to dylei@polyu.edu.hk

Dr. Y. Gu, Prof. Dr. W.-T. Wong

Department of Applied Biology and Chemical Technology, The Hong Kong Polytechnic University, Hong Kong

Keywords: molybdenum sulfide (MoS_2), nanodots and nanosheets, two-photon absorption, two-photon luminescence, multiphoton bioimaging

Abstract: Molybdenum disulfide nanodots (MoS_2 NDs) exhibit exotic optical, electronic, and catalytic properties, but so far limited understanding of their nonlinear optical properties has restricted wide applications in multiphoton bioimaging and nonlinear optoelectronics. In this work, we combine the two-photon luminescence (TPL) excitation and Z-scan spectroscopies to study the second order response of chemically prepared MoS_2 NDs and reveal, for the first time, that the efficient TPL occurs for the two-photon absorption (TPA) populated electrons from $1S_h$ to $1P_e$ through phonon-mediated relaxation to $1S_e$ excitonic state, followed by fast transition to the surface defect states. The strong excitation-wavelength dependence of both one-photon luminescence and TPL in MoS_2 NDs arises from the reabsorption effect and structural size inhomogeneity, distinctively different from their nanosheets counterpart that exhibits strong excitonic resonance enhanced second harmonic emission. Finally we demonstrate that the optimized excitation wavelength with a cross-section of 1.02×10^4 GM produces the highest-contrast multiphoton imaging of HeLa cells incubated with the MoS_2 NDs. The present nonlinear results have not only determined the precise amount of energy splitting between $1S_e$ and $1P_e$ but also offered critical criterion for optimizing the TPL-based multicolor cellular imaging performance with MoS_2 NDs probes.

Sun, J., Gu, Y. J., Lei, D. Y., Lau, S. P., Wong, W. T., Wong, K. Y., & Chan, H. L. W. (2016). Mechanistic understanding of excitation-correlated nonlinear optical properties in MoS2 nanosheets and nanodots: the role of exciton resonance. ACS photonics, 3(12), 2434-2444.

1. Introduction

As an exciting transition metal dichalcogenide crystal (TMDC), molybdenum disulfide (MoS_2) has attracted great research interest due to its exotic optical, electronic, and catalytic properties.[1-4] In sharp contrast to the most well-known two-dimensional (2D) material - graphene having a zero bandgap, monolayer MoS_2 is a direct bandgap semiconductor with an energy gap of 2.41 eV and thus can be used as an optically active layer in making light emitting diodes,[5] switchable transistors[6, 7] and photodetectors.[8] Due to this intrinsic nature, the photoluminescence (PL) quantum efficiency of a freestanding MoS_2 monolayer can be 10^4 times higher than its bulk counterpart (having an indirect bandgap of 1.29 eV).[1, 9] However, the efficient luminescence was only observed in monolayer MoS_2 and the emission energy of a pristine monolayer is untunable in the absence of an external field stimulus. Additionally, a MoS_2 monolayer absorbs only a very small portion of the incident light energy (< 11%) because of its ultrathin thickness.[10] The fixed emission-energy and low absorption-efficiency of MoS_2 monolayers have incurred many unfavorable limitations in optoelectronic device applications, particularly in the aspect of flexible control over their emission properties.

Recently, a great deal of research attention has been focused on zero-dimensional MoS_2 nanodots (NDs) less than 10 nm in diameter. MoS_2 NDs are fundamentally different from their bulk and 2D counterparts both in terms of their structures and photoelectrical properties. Three-dimensional (3D) spatial confinement and stronger surface effects in MoS_2 NDs enable fully altering their optical and electronic properties by controlling their diameters.[11] For example, MoS_2 NDs exhibit strong visible luminescence with PL quantum yield up to 19% and their emission wavelength highly depends on the excitation wavelength varied from ~320 to 500 nm,[12-15] drastically different from 2D few-layered MoS_2. More interestingly, strong

two-photon luminescence (TPL) has also been observed in MoS_2 NDs and applied in high-contrast bioimaging.[13-16]

Although surface defects are commonly considered to be responsible for the excitation wavelength dependent PL observed in MoS_2 NDs, synthesized by either sulfuric acid-assisted ultrasonic methods[16] or hydrothermal approaches,[12-15] the exact physical mechanisms of excitation-tunable PL and particularly efficient TPL remain poorly understood. When electron-hole pairs in a semiconductor are confined in real space, they generally follow Heisenberg's uncertainty principle such that their position in the *k*-space is blurred.[17, 18] This indicates that the tails of the electron and hole wave functions can partially overlap even in an indirect bandgap semiconductor, giving rise to quasi-direct transitions and thus increasing the probability of radiative recombination of excited carriers. However, the validity of describing the electronic properties of MoS_2 NDs by means of a band structure remains a question because the system of NDs has a much lower level of translational symmetry. Additionally, previous experimental and theoretical studies on improving the fundamental understanding of the two-photon absorption (TPA) in colloidal nanocrystals, such as lead-salt quantum dots, have revealed that quantum confinement could alleviate the strict requirement by optical selection rules.[19] This can give rise to one-photon allowed transitions in TPA and vice versa. Nevertheless, TPL excitation spectroscopy has not been carried out yet to probe the electronic band structure of, and understand, the spectral dependence of TPA in MoS_2 NDs. The latter is expected to provide important guidelines for selecting appropriate two-photon excitation wavelengths to optimize the TPL-based cellular imaging performance.

By combining the excitation wavelength and power dependent PL and TPL spectroscopic measurements, here we have, for the first time, revealed a full scenario of the observed wavelength-dependent TPL in MoS_2 NDs: initial population of

electrons at the 1P excitonic state and subsequent phonon-assisted relaxation to 1S, followed by a transition to the surface defect states. Our power dependent TPL and Z-scan measurements have unambiguously confirmed the second order response of the MoS_2 NDs and quantitatively determined their TPA cross section. The present nonlinear measurement results have not only determined precisely the amount of energy splitting between the $1S_e$ and $1P_e$ excitonic states but also offered critical criterion for optimizing the performance of TPL-based multicolor cellular imaging with MoS_2 NDs probes.

2. Results and discussion

2.1 Synthesis and characterization of MoS_2 NDs and nanosheets (NSs)

The MoS_2 NDs studied in this work were prepared by grinding a bulk MoS_2 crystal, followed with sonication, centrifugation and solvothermal treatment in N,N-dimethylformamide (DMF) solution. As illustrated in Scheme 1, a bulk MoS_2 crystal possesses a planar, covalently-bonded S-Mo-S sandwich structure and consecutive layers are stacked through weak van der Waals interaction. To obtain small sized MoS_2 NDs, both interlayer stacking and in-plane S-Mo-S bonds have to be broken. The combination of grinding and sonication, as a typical top-down approach, can weaken the van der Waals interaction in the bulk MoS_2 and results in few-layered MoS_2 NSs and even layered MoS_2 NDs under more intensive grinding and sonication.[16, 20] However, this method is inefficient in producing high-yield MoS_2 NDs in solution phase and also requires the use of dedicated facilities, making the high-yield production of MoS_2 NDs challenging up to now. Here we have combined this well-known method with a hydrothermal process, where the hydrodynamic force resulting from increased pressure and temperature leads to efficient breaking up of the in-plane S-Mo-S bonds and thus effective cutting of MoS_2

NSs into smaller sized MoS_2 NDs. The synthesis mechanism shares close similarities to that for graphene NDs synthesis where degradation of layered graphene dispersions was accelerated with hydrothermal or solvothermal treatment.[21, 22]

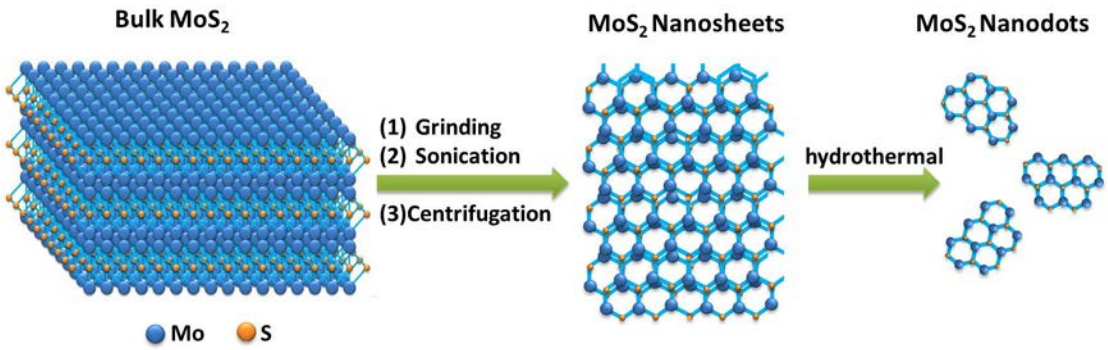

Scheme 1 Schematic procedures for synthesis of MoS_2 NDs from bulk MoS_2 crystal.

Transmission electron microscopy (TEM) imaging was performed to characterize the morphology and determine the size distribution of the as-prepared MoS_2 NSs and NDs. As seen in **Figure 1**a, the lateral size of the layered MoS_2 NSs is on the order of sub-100 nm and a number of ultrathin NSs can be observed in the TEM image shown in **Figure S1**. The high-resolution TEM (HRTEM) image in **Figure 1**b reveals the formation of nanoporous structures at the edges of NSs, possibly due to scission induced by extensive grinding and sonication, and these nonporous structures are energetically preferable to further break into smaller MoS_2 NDs at high temperature, enabled by the hydrodynamic force induced rupture of the S-Mo-S bonds. As shown in **Figure 1**d, uniform and monodispersed MoS_2 NDs with average diameter of ~4.8 nm (see the histogram statistics in **Figure 1**g) were produced after the post solvothermal treatment. As measured from the HRTEM image in Figure 1e, the lattice constant of the selected MoS_2 ND is 0.27 nm, corresponding to the (100) plane of the hexagonal MoS_2 crystal with six-fold symmetry.[14, 15] **Figure 1**f shows a

polycrystalline-like selected area electron diffraction (SAED) pattern captured for randomly oriented MoS_2 NDs, corresponding to continuous appearance of the six individual points observed for the (100) and (110) planes in the MoS_2 NSs in **Figure 1**c. Raman spectroscopy was conducted to confirm the atomic structural arrangement of MoS_2. The measured Raman spectra shown in **Figure 1**h demonstrate that both MoS_2 NSs and NDs exhibit two characteristic Raman bands at around 382.2 and 408.9 cm^{-1} as observed in the bulk MoS_2, assigned as the in-plane (E^1_{2g}) and out-of-plane (A_{1g}) vibrational modes of the 2H-MoS_2 crystal.[16] A mean frequency difference in the two characteristic bands is 24.3 and 23.6 cm^{-1} for MoS_2 NSs and MoS_2 NDs, respectively, both of which are slightly smaller than that for the bulk MoS_2 (26.7 cm^{-1}). In addition, the spectral broadening observed in the E^1_{2g} and A_{1g} bands of the NSs and NDs, in comparison with that of the bulk MoS_2, indicates significant reduction in the flake thickness and lateral size from the bulk form to the dispersed counterparts. Thickness of the NSs and NDs?.

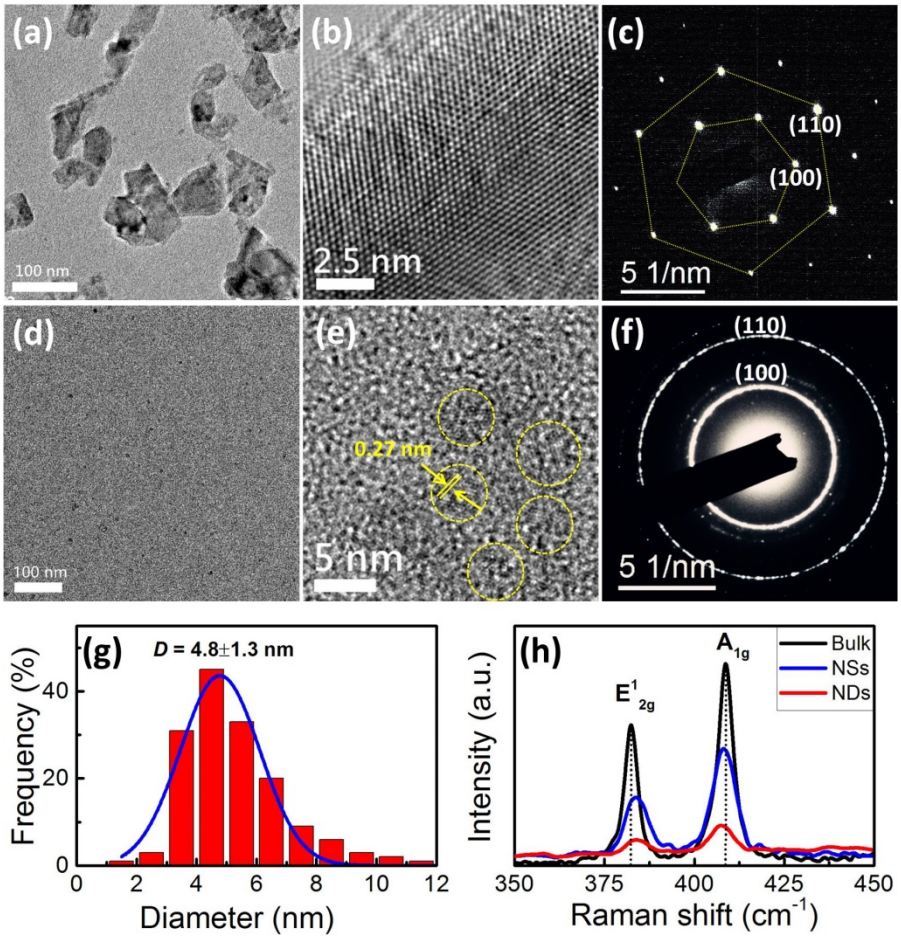

Figure 1 Transmission electron microscopy (TEM) images of (a) MoS_2 NSs and (d) MoS_2 NDs. High-resolution TEM images of (b) few-layered MoS_2 NSs and (e) NDs. Selected area electron diffraction patterns of (c) MoS_2 NSs and (f) NDs. (g) Size distribution of MoS_2 NDs and (h) Raman spectra of bulk MoS_2, NSs and NDs measured at excitation wavelength of 532 nm.

2.2 Linear and nonlinear optical properties of MoS_2 NDs and NSs

The UV–Vis absorption spectra of the prepared MoS_2 NSs and NDs in DMF solution are shown in **Figure 2**a. Four characteristic absorption bands are observed in the spectrum of MoS_2 NSs, consistent with previous reports.[12, 14] The distinct absorption peaks A and B (labeled according to earlier convention) correspond to the excitonic transitions occurring at the K/K′ points of the first Brillouin zone while the peaks C and D are assigned to the direct transitions from the deep valence band to the conduction band.[1] In the scenario of single-electron band structure, these four

excitonic transitions occur in the region of the first Brillouin zone where the valence and conduction bands are nested. However, the absorption spectrum of the MoS_2 NDs exhibits no characteristic absorption peaks in the measured wavelength region and only an absorption edge is observed at ~415 nm, revealing an optical bandgap larger than 3.0 eV. On the one hand, the observed blueshift in the absorption edge of the MoS_2 NDs compared to that of the MoS_2 NSs could be qualitatively explained due to stronger quantum confinement effect in the NDs. On the other hand, it has been widely reported that discrete electronic states can be masked in the linear optical absorption response of chemically-grown semiconductor NDs due to structural inhomogeneity induced spectral broadening [23, 24] because the NDs could vary in size, geometry, and stoichiometry. In our study, the MoS_2 NDs may have even more complicated lattice imperfections because of the lattice distortion and deviation from stoichiometry induced by the solvothermal treatment. Therefore, not only surface states but also intrinsic defects are equally important to the absorption response of the MoS_2 NDs and both can act as potential structural defects to localize photo-excited charge carriers. As a result, both structural inhomogeneity and defects in the MoS_2 NDs smear out the excitonic absorption peaks originally observed in the MoS_2 NSs.

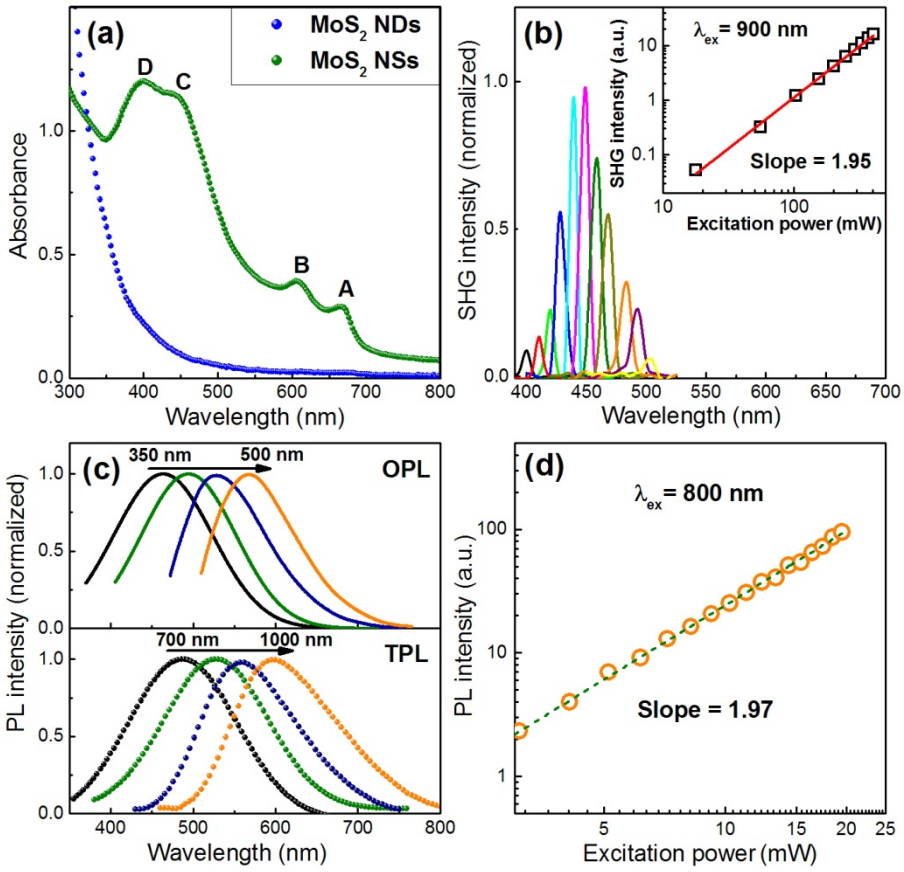

Figure 2 (a) UV–Vis absorption spectra of the MoS_2 NSs and MoS_2 NDs in DMF solution. (b) Normalized optical SH emission spectra of the NSs measured at different excitation wavelengths (800 – 1010 nm) with fixed power (50 mW). The inset shows a double-logarithmic plot of the SH emission intensity (open squares) as a function of excitation power as well as the linear fit (solid line) to the experimental data. (c) OPL and TPL spectra of the NDs at different excitation wavelengths, 350 – 500 nm for OPL and 700 – 1000 nm for TPL, respectively. (d) Double-logarithmic plot of the TPL signal intensity (open circles) as a function of excitation power measured at 800 nm as well as the linear fit (dashed line) to the experimental data.

Strikingly, the MoS_2 NSs and NDs prepared here exhibit not only peculiar optical absorption properties, as shown above, but also distinctive nonlinear emission properties: the former shows efficient second harmonic generation (SHG) while the latter exhibits bright TPL, both with strong excitation wavelength dependence. **Figure 2**b shows the excitation wavelength dependent SH emission spectra for the MoS_2 NSs and the inset renders the excitation power dependent SH emission intensity at

wavelength 900 nm, where a linear fit to the experimental data generates a slope of 1.95, confirming the second-order nature of the measured emission signals. Over the scanning wavelength range from 800 to 1010 nm, we observe a significant variation in the SH emission intensity, with a maximum appearing at the excitation wavelength of 900 nm, where the corresponding two-photon excitation energy (450 nm) is in resonance with the C-exciton absorption peak as shown in **Figure 2**a. The observed exciton resonance enhanced SHG can be attributed to the combination of electric dipole and magnetic dipole transitions in the MoS_2 NSs, sharing a similar scenario as that observed in *h*-BN and MoS_2 monolayers.[25]

Remarkably different from the MoS_2 NSs, the MoS_2 NDs show strong excitation wavelength dependent one- and two-photon luminescence (OPL and TPL, see **Figure 2**c). Similar to previous reports,[12-15] the OPL (TPL) peak shifts from 450 to 570 nm (from 480 to 595 nm) as the excitation wavelength increases from 350 to 500 nm (from 700 to 1000 nm), sharing close similarities to the emission properties of graphene NDs.[21] The observed emission tunability could be a result of the large size variation and different emissive sites on the surface of the MoS_2 NDs. In addition, both OPL and TPL spectra have a broad emission band with a full width at half maximum (FWHM) of more than 100 nm, comparable to that of graphene quantum dots[21, 22] but almost four times that of conventional semiconductor quantum dots such as monodispersed CdSe.[26] The significantly broadened emission linewidth of the MoS_2 NDs are mainly due to the wide distribution of lattice vibrational states and structural size inhomogeneity. More surprisingly, the low-energy tail of the OPL band extends much below the absorption edge of the NDs, and even beyond the A-exciton absorption peak of the NSs. This indicates that the radiative transition in the NDs does not come from band edge or excitonic recombination. In fact, all the emission features including wide tunability, broad linewidth and extended tail are characteristics of

structural defects related carrier recombination. This speculation is further verified by the observation that both OPL and TPL peaks of the MoS_2 NDs exhibit a large Stokes-shift around ~0.45 eV, with respect to the corresponding excitation energy. Finally, to confirm the TPL signal originates from two-photon absorption (TPA), we measured the integrated TPL intensity as a function of excitation power at wavelength 800 nm, with results shown in **Figure 2**d, demonstrating a clear quadratic dependence (slope of 1.97).

2.3 Mechanistic understanding of excitation-correlated TPL of MoS_2 NDs

Based on the above experimental observations, we can now provide a more comprehensive microscopic understanding on the emission properties of the MoS_2 NDs. On the one hand, in the sub-5 nm NDs many atoms locate at, or near, the surface where the surface states associated with adsorbed species, dangling bonds and structural defects are present, and these bound states are expected to play an important role in the decay behavior of photo-induced charge carriers. These surface trapping states that are individually incorporated into solid hosts lead to excitation wavelength dependent multicolor emissions as observed in experiment, and the emission energy must be smaller than the bandgap energy. Because of the larger effective mass of holes than electrons in MoS_2, the hole-related traps are generally located much deeper than the electron-related counterparts, and the finite distribution of their energies and depth locations is responsible for the observed broad emission bands. In general, a deeper hole-related trap has an emission peak redshifted compared to a shallow electron-related one. On the other hand, a careful comparison of the measured OPL and TPL spectral profile provides more important insights into the nonlinear emission mechanism of the MoS_2 NDs. No significant difference can be seen in the spectral profile of OPL and TPL, except a red shift in the peak wavelength. This indicates that

the OPL and TPL observed in the MoS_2 NDs come from the same radiative recombination channel, and thus they share similar spectral features such as wide emission tunability and broad emission linewidth. The persistent red shift in the TPL peak compared to the corresponding OPL can be attributed to reabsorption effect and structural size inhomogeneity, and this has been widely observed in conventional semiconductor quantum dots as well.[27]

Once we have understood both linear and nonlinear emission properties of the MoS_2 NDs, we then combine the OPL and TPL excitation (OPLE and TPLE) spectroscopies to explore their linear and nonlinear absorption behaviors in order to fully determine their band structures and detailed electronic structures. In the past, the TPLE spectroscopy was successfully used to probe the excitonic dark states in TMDC monolayers[28] and carbon nanotubes.[29] The low-energy states of the confined electrons and holes in the MoS_2 NDs are shown in **Figure 3**b, where the labels s and p correspond to the states with angular momentum $l = 0$ and 1, while the indices e and h denote electron and hole. In accordance with the electric dipole approximation,[27] one- and two-photon allowed absorption transitions in quantum dots satisfy the selection rules $\Delta l = l_f - l_i = 0$ and ± 1, respectively, where l_f and l_i are the orbital quantum numbers of the final and initial electronic states. Note that the respective selection rules in 3D-confiend quantum dots are different from that for bulk or 2D semiconductors because the system of quantum dots has a much lower level translational symmetry.[28-30] Although the OPA and TPA bands of a real nanoscale system can be broadened to a great extent due to structural size inhomogeneity, it is expected that the difference in their energies can be observed. In our experiment, the integrated TPL signal intensity was collected while scanning the excitation laser energy from 1.77 eV to 1.19 eV, with the TPL excitation spectrum shown in **Figure 3**a and compared with the OPL excitation spectrum. As shown in **Figure 3**a, the MoS_2

NDs present a resonant TPL excitation band centered at 3.3 eV corresponding to the lowest energy of two-photon allowed excitonic transition ($1S_h \rightarrow 1P_e$). The peak of the TPL excitation spectrum locates at an energy higher that of the OPL excitation peak arising from the first excitonic transition of $1S_h \rightarrow 1S_e$. Remarkably, a blue shift of 0.3 eV, which can be defined as the energy difference between $1S_e$ and $1P_e$ electronic states in the MoS_2 NDs, is observed by comparing the OPL and TPL excitation spectra. This energy splitting is larger than the reported value of 0.21 eV for MoS_2 monolayers[30] and the enlarged splitting can be attributed to stronger quantum confinement effect in the MoS_2 NDs. In connection with the emission properties discussed above, we can now for the first time conclude that the absorption in MoS_2 NDs is mediated by excitonic states while the emission is due to the radiative transition from band states to surface states.

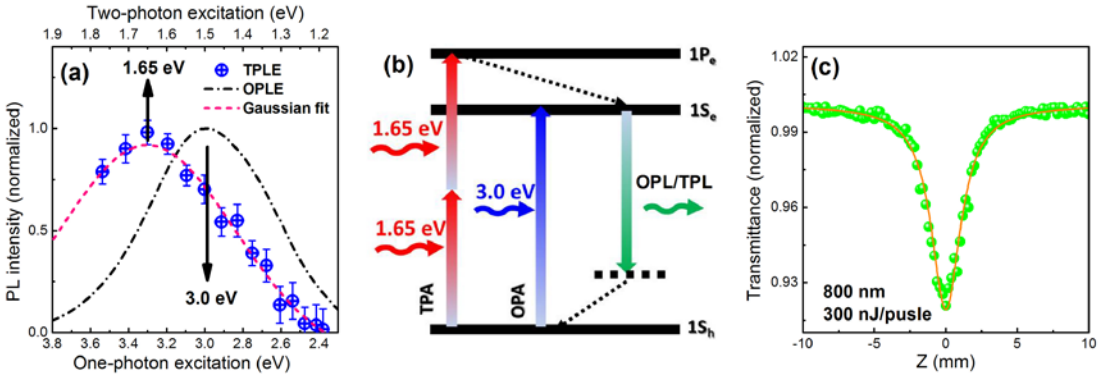

Figure 3 (a) Comparison of the OPLE (black line) and TPLE (blue circles) spectra for MoS_2 NDs at a detection wavelength of 520 nm. TPLE spectrum (red line) was obtained by Gaussian fitting. The error bars represent the standard deviation of the measured laser powers. (b) Schematic illustration of the near-gap energy levels and one- and two- photon allowed dipole-transitions in MoS_2 NDs. (c) Open aperture Z-scan responses of MoS_2 NDs solution. The red curve is the best-fitting curve according to Z-scan theory.

In order to quantitatively determine the TPA cross section of the MoS_2 NDs in DMF solution, we performed an open-aperture Z-scan measurement by translating the

sample through the focal plane of a focused Gaussian laser beam while monitoring the change in the transmission intensity.[31] Note that the TPA cross-section of DMF is negligible and has no influence in the nonlinear absorption of the MoS_2 NDs. **Figure 3**c shows the measured transmittance as a function of the sample location relative to the focal plane at excitation energy of 300 nJ/pulse, the Z-scan fitting of which gives rise to a TPA coefficient of 0.016 cm/GW for the MoS_2 NDs at concentration 2.35 mg/mL. Correspondingly, the TPA cross-section (σ_{TPA}) of the MoS_2 NDs is estimated to be 1.02×10^4 GM at wavelength of 800 nm, comparable to the recently reported value of 9800 GM.[15] This value is much larger than that of conventional dyes and comparable to, or even bigger than, that of Cd based quantum dots,[27] making MoS_2 NDs a very promising candidate as nonlinear optical probes in TPL based bioimaging applications.

2.4 Optimum TPL-based multicolor cellular-imaging

Inspired by the observed highly-efficient and excitation-correlated TPL, we attempt to explore multicolor-TPL cell imaging with the prepared MoS_2 NDs. Before carrying out the cellular imaging, the cytotoxicity of the MoS_2 NDs in HeLa cells was evaluated by MTT assay. As shown in **Figure 4**a, the viability of the cells after exposed to 0.72 mg/mL of MoS_2 NDs for 24 h remained greater than 90%, demonstrating a relatively low toxicity of the MoS_2 NDs. These results indicate that MoS_2 NDs do not obviously inhibit the proliferation of the cells, confirming that they are suitable for biomedical applications. Confocal laser scanning microscopy (CLSM) was used to further demonstrate the cell permeability and bioimaging of MoS_2 NDs. **Figures 4**b-d show the TPL images of HeLa cells incubated with the MoS_2 NDs, under excitation at 750, 850 and 950 nm, respectively. The highest contrast image, clearly outlining the cell profile, was obtained under 750 nm excitation (see **Figure**

4b), consistent with the TPLE peak observed in Figure 3a. This multi-color TPL imaging with the MoS_2 NDs has a great advantage over other labeling agents – offer more degrees of freedom in selecting desired excitation wavelength for observation. The merged image (**Figure 4**f) of fluorescence image (blue, **Figures 4**b) and bright field (**Figure 4**e) demonstrates that the MoS_2 NDs can simultaneously label both membrane and cytoplasm of the HeLa cells without photobleaching. The low toxicity, good biocompatibility, broad tunability and remarkably high photostablity of the MoS_2 are beneficial for bioimaging and detection in deep tissue.

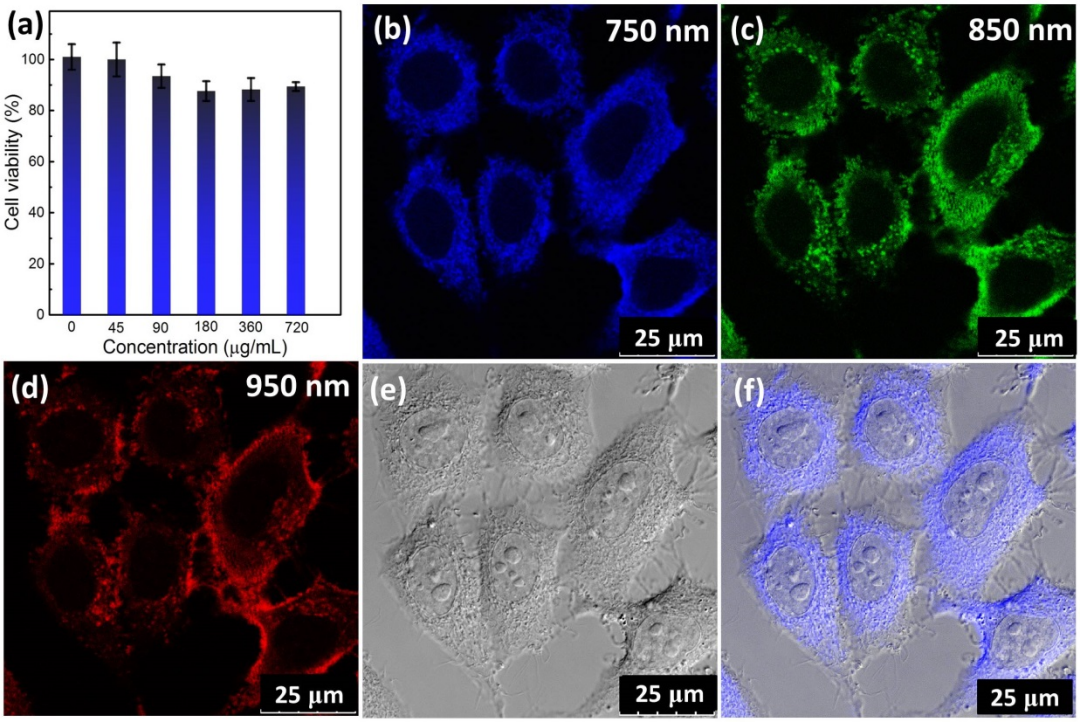

Figure 4 (a) Cell viability after 24 h incubation with concentration-varied MoS_2 NDs. Each data point represents mean ± SD from 5 trials. (b-d) Two-photon confocal microscope images of the HeLa cells captured under excitation wavelength (b) 750 nm, (c) 850 nm, and (d) 950 nm. The TPL signals for the three images were filtered respectively by three band pass filters within the range 480-520 nm (b), 520-560 nm (c) and 560-600 nm (d). (e) Bright field image. (f) The merged bright field and TPL image of the HeLa cells**.** The cells were incubated with 0.36 mg/mL MoS_2 NDs for 24 h at 37 ^oC.

3. Conclusion

In summary, we have investigated the nonlinear TPL and TPA properties of chemically prepared MoS_2 NDs. Our results have provided the first mechanistic understanding of the exciton-assisted TPA and surface defects related TPL in the MoS_2 NDs, successfully explaining the emission color tunability and broad emission linewidth. Finally, we have demonstrated that the MoS_2 NDs with large TPA cross-section and bright excitation-correlated TPL can be used as a promising probe for multi-color cellular imaging with excellent biocompatibility and flexible selection of both excitation and detection wavelengths.

4. Experimental Section

Chemical Materials: MoS_2 powders, DMF and MTT were purchased from Sigma–Aldrich Corporation (China). All reagents were of analytical grade and used without further purification.

Synthesis of MoS_2 NDs: MoS_2 NSs were prepared first. Briefly, 200 mg MoS_2 powder were dispersed in DMF in a mortar with initial concentration of 200 mg/ml. After grinding for 1 h in a chemical hood, the dispersion was transferred to a glass vial containing 20 ml DMF solution, followed by sonication for 3 h at the power of 320 W at room temperature. The resultant dispersion was first centrifuged at 3000 rpm for 10 min. The yielded yellow-green supernatant was MoS_2 NSs. Then the top 2/3 of the dispersion, that is MoS_2 NSs solution, was decanted into a two-neck bottle and kept vigorous stirring for 6 h at 110 °C. The resultant dispersion was then purified by centrifugation and filtration. The suspension was first centrifuged at 7500 rpm for 10 min. After that, the supernatant was gently transferred from the top dispersion and then filtered by a PTFE filter with pore size of 0.1 μm. Finally, the filtered MoS_2 NDs

were collected in a clean glass vial for further characterization.

Characterization: The size distribution of MoS_2 NDs was determined by transmission electron microscopy (TEM) (JEM-2010F from JEOL, 200 KV). Raman spectra were recorded on a Laser Raman spectrometer (NT-MDT, NTEGRA Spectra) equipped with 532 nm semiconductor laser and charge-coupled device (DU420A, Andor) detector. Steady-state absorption spectra were recorded by means of a UV-vis-NIR scanning spectrophotometer (UV-2550, Shimadzu). One-photon induced luminescence spectroscopy was carried out with a spectrophotometer (FLS920, Edinburgh Instruments). Two-photon induced luminescence and SHG spectroscopy was carried out by a Leica SP8 multiphoton microscope equipped with a mode-locked Ti:Sapphire laser (MaiTai, Spectra Physics) with pulses of 100 fs at a repetition rate of 80 MHz.

Z-scan spectroscopy and Two-photon excitation spectroscopy: An open-aperture Z-scan system based on a regeneratively amplified mode-locked Ti:sapphire laser operating at 800 nm, 50 fs pulses width, with repetition rate of 1 kHz was employed to study the ultrafast TPA behavior of the MoS_2 NDs dispersions. The reference beam of incident light and the transmitted beam were monitored by two photodiodes as the sample moved through the focus of a lens along the laser propagation direction. The two-photon excitation spectroscopy is carried out on Leica SP8 multiphoton microscope with a mode-locked Ti:Sapphire laser (MaiTai, Spectra Physics) with pulses of 100 fs at a repetition rate of 80 MHz. The two-photon emission intensities are normalized to the square of the focused power, as the excitation power is limited to the unsaturated regime.

***Cytotoxicity of MoS_2 NDs*:** Before cytotoxicity evaluation, the MoS_2 NDs in DMF solution was evaporated to completely remove the DMF solvent and redispersed in

water for further use. The cells cytotoxicity of MoS_2 NDs was tested on HeLa cells, which was referred to our previous work. Typically, HeLa cells were routinely cultured in flasks and incubated at 37 ^oC in a humidified hood incubator set at 5% CO_2 atmosphere. To determine cell cytotoxicity/viability, the cells were plated at a density of 1×10^4 cells / well in a 96-well plate. After 24 h, the cells were exposed to different concentrations of MoS_2 NDs (0.045, 0.09, 0.18, 0.36, 0.72 mg mL^{-1}) and incubated for 24 h. The same volume of PBS was set as the negative control and the cell culture medium was set as the blank control. The cell viability after exposed to MoS_2 NDs was compared to that of the negative control. The treatment medium was removed after co-incubation and 150 mL of thiazolyl blue tetrazolium bromide (0.5 mg/mL in phosphate buffer pH 7.4, MTT, Sigma-Aldrich) was added to each well. After 4 h of co-incubation, the MTT medium was removed and formazan crystals were solubilized with 100 ㎖ of DMSO and ethanol (1:1), and the solution was vigorously mixed to dissolve the reacted dye. The absorbance was read on a microplate reader at 570 nm. The relative cell viability (%) of the cells exposed to was determined by comparing their absorption with control cells.

Multicolor cellular-imaging: A Leica SP8 multiphoton microscope was used for TPL imaging of HeLa cells incubated with MoS_2 NDs. A mode-locked Ti:Sapphire laser (MaiTai, Spectra Physics) with pulses of 100 fs at a repetition rate of 80 MHz was used as the excitation source. For cellular imaging, Hela cells were cultured in modified Eagle's medium supplemented with 10% fetal bovine serum and 1 % penicillin/streptomycin (DMEM) using glass bottom dish (Mattek). All cells were incubated at 37 ^oC in a CO_2 incubator until approximately 50 % confluence was reached. The aqueous solution of the MoS_2 NDs (10 mg/mL, 0.2 mL) was mixed with the culture medium (1.8 mL) and was added in Hela cells. After incubation for 20 h,

the Hela cells were washed three times with PBS (1 mL) and kept in PBS for two-photon imaging on the SP8 multiphoton microscope with excitation at 750 nm, 850 nm and 950 nm using a 63× oil immersion objective lens.

Supporting Information

Supporting Information is available from the Wiley Online Library or from the author.

Acknowledgements

The authors acknowledge the financial support by the Hong Kong Polytechnic University (Grant Nos. 1-ZVAW and 1-ZVCG) and the Hong Kong Research Grants Council (GRF Grant No. 153014). Dr. Jianhui Sun thanks Mr. Decheng Yang for his assistance in the Z-scan measurement.

References

[1] K. F. Mak, C. Lee, J. Hone, J. Shan, T. F. Heinz, *Phys. Rev. Lett.* **2010**, 105, 136805.

[2] H. I. Karunadasa, E. Montalvo, Y. Sun, M. Majda, J. R. Long, C. J. Chang, *Science* **2012**, 335, 698.

[3] Q. H. Wang, K. Kalantar-Zadeh, A. Kis, J. N. Coleman, M. S. Strano, *Nat. Nanotechnol.* **2012**, 7, 699.

[4] R. Cheng, S. Jiang, Y. Chen, Y. Liu, N. Weiss, H.C. Cheng, H. Wu, Y. Huang, X. Duan, *Nat. Commun.* **2014**, 5, 5143.

[5] R. Cheng, D. Li, H. Zhou, C. Wang, A. Yin, S. Jiang, X. Duan, *Nano Lett.* **2014**, 14, 5590.

[6] S. Kim, A. Konar, W. S. Hwang, J. H. Lee, J. Lee, J. Yang, Y. W. Jin, *Nat. Commun.* **2012**, 3, 1011.

[7] B. Radisavljevic, A. Radenovic, J. Brivio, V. Giacometti, A. Kis, *Nat. Nanotechnol.* **2011**, 6, 147.

[8] O. Lopez-Sanchez, D. Lembke, M. Kayci, A. Radenovic, A. Kis, *Nat. Nanotechnol.* **2013**, 8, 497.

[9] G. Eda, H. Yamaguchi, D. Voiry, T. Fujita, M. Chen, M. Chhowalla, *Nano Lett.*

2011, 11, 5111.
[10] J. T. Liu, T. B. Wang, X. J. Li, N. H. Liu,. *J. Appl. Phys.* **2014**, 115, 193511.
[11] J. O. Joswig, T. Lorenz, T. B. Wendumu, S. Gemming, G. Seifert, *Acc. Chem. Res.* **2014**, 48, 48.
[12] D. Gopalakrishnan, D. Damien, M. M. Shaijumon, *ACS Nano* **2014**, 8, 5297.
[13] H. Dong, S. Tang, Y. Hao, H. Zhu, W. Dai, G. Zhao, Y. Cao, H. Lu, X. Zhang, J. Ju, *ACS Appl. Mater. Interfaces* **2016**, 8, 3107-3114.
[14] S. Xu, D. Li, P. Wu, *Adv. Funct. Mater.* **2015**, 25, 1127.
[15] W. Gu, Y. Yan, X. Cao, C. Zhang, C. Ding, Y. Xian, *J. Mater. Chem. B* **2016**, 4, 27.
[16] W. Dai, H. Dong, B. Fugetsu, Y. Cao, H. Lu, X. Ma, X. Zhang, *Small* **2015**, 11, 4158.
[17] J. P. Wilcoxon, G. A. Samara, *Phys. Rev. B* **1995**, 51, 7299.
[18] V. Kocevski, O. Eriksson, J. Rusz, *Phys. Rev. B* **2013**, 87, 245401.
[19] G. Nootz, L. A. Padilha, P. D. Olszak, S. Webster, D. J. Hagan, E.W.V. Stryland, L. Levina, V. Sukhovatkin, L. Brzozowski, E. H. Sargent, *Nano Lett.* **2010**, 10, 3577.
[20] X. Zhang, Z. Lai, Z. Liu, C. Tan, Y. Huang, B. Li, M. Zhao, L. Xie, W. Huang, H. Zhang, *Angew. Chem. Int. Ed.* **2015**, 127, 5515.
[21] D. Pan, J. Zhang, Z. Li, M. Wu, *Adv. Mater.* **2010**, 22, 734.
[22] H. Tetsuka, R. Asahi, A. Nagoya, K. Okamoto, I. Tajima, R. Ohta, A. Okamoto, *Adv. Mater.* **2012**, 24, 5333.
[23] V. I. Klimov, S. Hunsche, H. Kurz, *Phys. Rev. B* **1994**, 50, 8110.
[24] J. Sun, D. Zhu, J. Zhao, M. Ikezawa, X. Wang, Y. Masumoto, *Appl. Phys. Lett.* **2014**, 104, 023118.
[25] G. Wang, X. Marie, I. Gerber, T. Amand, D. Lagarde, L. Bouet, M. Vidal, A. Balocchi, B. Urbaszek, *Phys. Rev. Lett.* **2014**, 89, 081102.
[26] J. L. Zhao, J. A. Bardecker, A. M. Munro, M. S. Liu, Y. H. Niu, I. K. Ding, J. D. Luo, B. Q. Chen, A. K.-Y. Jen, and D. S. Ginger, *Nano Lett.* **2006**, 6, 463.
[27] M. Allione, A. Ballester, H. Li, A. Comin, J. L. Movilla, J. I. Climente, L. Manna, I. Moreels, *ACS nano* **2013**, 7, 2443
[28] F. Wang, G. Dukovic, L. E. Brus, T. F. Heinz, *Science* **2005**, 308, 838.
[29] Z. Ye, T. Cao, K. O'Brien, H. Zhu, X. Yin, Y. Wang, S. G. Louie, X. Zhang, *Nature* **2014**, 513, 214.
[30] T. C. Berkelbach, M. S. Hybertsen, D. R. Reichman, *Phys. Rev. B* **2015**, 92, 085413.
[31] S. Zhang, N. Dong, N. McEvoy, M. O'Brien, S. Winters, N. C. Berner, C. Yim, Y. Li, X. Zhang, Z. Chen, L. Zhang, G. S. Duesberg, J. Wang, *ACS nano* **2015**, 9, 7142.

Molybdenum disulfide nanodots (MoS_2 NDs) were prepared and they exhibit excitation-correlated two-photon luminescence (TPL) ranging from 480 to 595 nm. The efficient TPL occurs for the two-photon absorption (TPA) populated electrons from $1S_h$ to $1P_e$ through phonon-mediated relaxation to $1S_e$ excitonic state, followed by fast transition to the surface defect states. The cellular imaging by MoS_2 NDs was undertaken to demonstrate the potential of these NDs as TPL-based multicolor probe.

Mechanistic Understanding of Excitation-Correlated Highly-Efficient Two-Photon Luminescence from Biocompatible MoS_2 Nanodots for Optimized Multicolor Cell Imaging

Jianhui Sun, Yanjuan Gu, Dang Yuan, Lei*, Siu Fung Yu, Shu Ping Lau, Wing-Tak Wong, Helen Lai-Wai Chan

Dr. J. Sun, Prof. Dr. D.Y. Lei, Prof. Dr. S.F. Yu, Prof. Dr. S.P. Lau, Prof. Dr. H.L.-W. Chan
Department of Applied Physics, The Hong Kong Polytechnic University, Hong Kong
Address correspondence to dylei@polyu.edu.hk
Dr. Y. Gu, Prof. Dr. W.-T. Wong
Department of Applied Biology and Chemical Technology, The Hong Kong Polytechnic University, Hong Kong

Keywords: molybdenum sulfide (MoS_2), nanodots and nanosheets, two-photon absorption, two-photon luminescence, multiphoton bioimaging

TOC figure

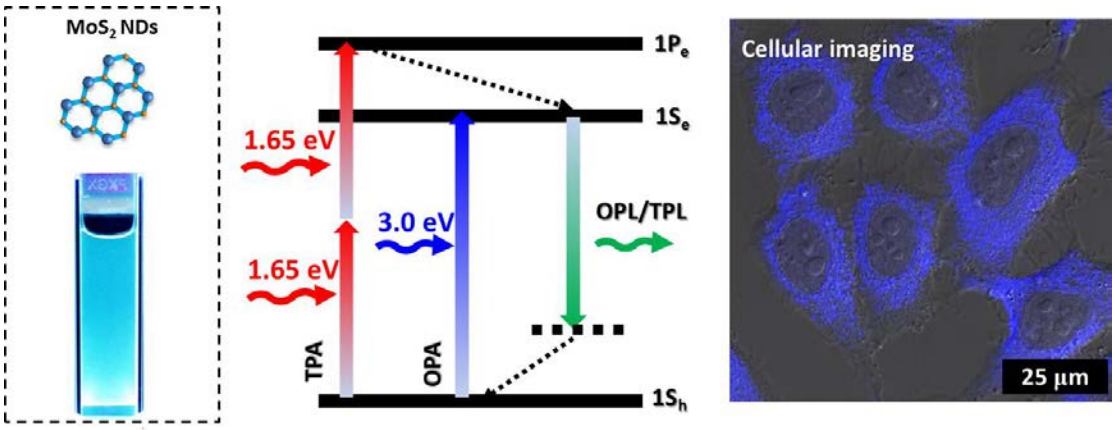

Supporting Information

Mechanistic Understanding of Excitation-Correlated Highly-Efficient Two-Photon Luminescence from Biocompatible MoS_2 Nanodots for Optimized Multicolor Cell Imaging

Jianhui Sun, Yanjuan Gu, Dang Yuan, Lei*, Siu Fung Yu, Shu Ping Lau, Wing-Tak Wong, Helen Lai-Wai Chan

Dr. J. Sun, Prof. Dr. D.Y. Lei, Prof. Dr. S.F. Yu, Prof. Dr. S.P. Lau, Prof. Dr. H.L.-W. Chan
Department of Applied Physics, The Hong Kong Polytechnic University, Hong Kong
Address correspondence to dylei@polyu.edu.hk
Dr. Y. Gu, Prof. Dr. W.-T. Wong
Department of Applied Biology and Chemical Technology, The Hong Kong Polytechnic University, Hong Kong

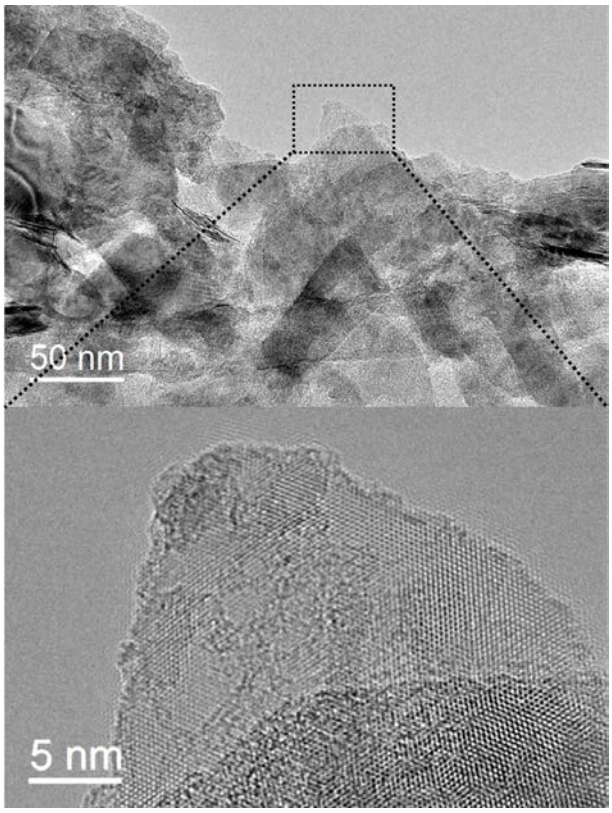

Figure S1 Transmission electron microscopy (TEM) images of MoS_2 NSs and high-resolution TEM images of the selected zone.